Hybrid Super-Nyquist CAP Modulation based VLC with Low Bandwidth Polymer LEDs

Paul Anthony Haigh[1,2], Petr Chvojka[3], Alessandro Minotto[4,5], Andrew Burton[6], Petri Murto[7],
Ergang Wang[7], Zabih Ghassemlooy[6], Stanislav Zvanovec[3], Franco Cacialli[4,5] and Izzat Darwazeh[2]

[1]*Intelligent Sensing and Communications Group, Newcastle University, UK*
[2]*Information and Communications Engineering Group, University College London, UK*
[3]*Department of Electromagnetic Field, Czech Technical University in Prague, Czech Republic*
[4]*Department of Physics and Astronomy, University College London, UK*
[5]*London Centre for Nanotechnology, University College London, UK*
[6]*Optical Communications Research Group, Northumbria University, UK*
[7]*Department of Chemistry and Chemical Engineering/Applied Chemistry,*
Chalmers University of Technology, Sweden
paul.haigh@newcastle.ac.uk

Abstract—**Visible light communication systems often suffer from high frequency attenuation when transmitting out-of-band. This effect has been ameliorated by multi-band modulations such as multi-band carrier-less amplitude and phase (m-CAP), which minimises the effect of decreased high frequency magnitude and maximises signal-to-noise ratio-per-sub-band. On the other hand, in the pass-band region, super-Nyquist CAP (SCAP) can offer throughput improvements with no additional complexity at the receiver, at the cost of bit error rate. We propose, for the first time, a new hybrid SCAP modulation format that takes advantageous of both SCAP (i.e. overlapped sub-bands within the modulation bandwidth) and conventional m-CAP (orthogonally spaced bands outside the modulation bandwidth) while maintaining isolation between noise sources. We show higher baud rates within the passband region whilst supporting out-of-band transmission at lower error vector magnitudes.**

Index Terms—**Carrier-less amplitude and phase modulation, digital signal processing, modulation, visible light communications**

I. INTRODUCTION

Polymer light-emitting diodes (PLEDs) represent an attractive alternative to conventional LEDs as the transmitter in visible light communications (VLC). PLED-based screens in smart devices can be used for (*i*) the uplink, a challenge in VLC where infrared [1] or radio frequencies [2] have typically been proposed; and (*ii*) embedding information onto the displayed image, thus allowing users to use the device as desired whilst still maintaining an active link. In our previous work [3], we showed that using organic PLEDs in a smart-display consisting of individual red-green-blue (RGB) pixels

capable of transmitting independent information could yield an advantage for a VLC uplink with an aggregated data rate of 55 Mb/s, which is generally sufficient for indoor applications.

However, one of the main problems with PLEDs is their inherently lower modulation bandwidth (typically in the order of hundreds of kHz) due to limited charge transport characteristics and large device area, which combined with sub-micron thickness result in high plate capacitances. This is a serious challenge for high-speed PLED-based VLC systems. In the literature, the vast majority of studies reported are focused on using pulse-amplitude modulation (PAM) with time-domain equalisation to overcome low bandwidth and increase speeds from several kb/s to 55 Mb/s [3, 4].

Alternatively, subcarrier modulation formats with high spectral efficiency such as orthogonal frequency division multiplexing (OFDM) [5], carrier-less amplitude and phase (CAP) modulation or multi-band CAP (m-CAP) [6], where m is the number of sub-bands (SBs), have been investigated to increase data rates. In [7], a comparative study of OFDM and CAP performed over an RGB-LED-based VLC link was carried out showing that 1-CAP (3.22 Gb/s) outperformed OFDM (2.93 Gb/s) in terms of data rate and bit-error rate (BER) performance. In [8, 9], it was shown that both the data rate and spectral efficiency improves with increasing m.

Recently, non-orthogonal modulation techniques such as spectrally efficient frequency division multiplexing (SEFDM) [10] and faster-than-Nyquist (FTN) signalling [11] have been investigated in VLC systems. These modulation formats are intended to improve the link capacity by intentionally introducing inter-carrier interference (ICI) or inter-symbol interference (ISI) in SEFDM and FTN, respectively. Note, the introduction of interference enables transmission of more symbols-per-second in the

same time period compared to conventional orthogonal systems. In [12], a non-orthogonal variation on m-CAP was proposed called super-Nyquist m-CAP (m–SCAP), where SBs are purposely overlapped reducing the total signal bandwidth and causing inter-band interference (IBI). Hence, higher symbol rates can be supported at the cost of BER. It was shown that 10-SCAP offered spectral efficiency improvement by ~45% with no additional digital signal processing at the receiver.

Therefore, considering the inherent low modulation bandwidth of PLEDs, m-SCAP could be an attractive modulation format for achieving a greater capacity. On the other hand, in VLC the signal bandwidth is generally higher than the modulation bandwidth, thus resulting in significant high frequency attenuation [13] i.e. higher BER. Hence, in this work, we propose and experimentally demonstrate a novel hybrid Super-Nyquist CAP modulation format including both super-Nyquist and orthogonal m-CAP, where the SBs placed in the pass- and stop-bands of the PLED frequency response are non-orthogonal and orthogonal, respectively. This is intended to separate the two dominant factors of IBI and high frequency attenuation in the super-Nyquist and orthogonal cases, respectively.

The rest of the paper is organised as follows; in Section II the proposed hybrid scheme is theoretically formulated and details of the fabrication and characterisation of the PLED under test as well as the VLC link details are provided. In Section III, measurement results are discussed and in Section IV conclusions are drawn.

II. HYBRID SUPER-NYQUIST CAP AND PLED

A. Hybrid Multi-Band CAP Modulator

The concept of hybrid super-Nyquist m-CAP (m-HSCAP) is shown in terms of the normalised magnitude responses of the transmit filters in Fig. 1 with 4 SBs, where the 1st two SBs are overlapped and 2nd two are orthogonally spaced. We selected a total transmission bandwidth of 1 MHz (i.e., the 1st two super-Nyquist SBs are located in the pass-band of the PLED frequency response $H(f)$ with a 3-dB modulation bandwidth of 500 kHz. Therefore, the 1st two SBs have a bandwidth of 312.5 kHz each in comparison to the 250 kHz bandwidth occupied by the 2nd two orthogonal SBs. Note, beyond the cut-off frequency the attenuation significantly increases (~10 dB/decade) due to the frequency response $H(f)$ of the PLED, see Fig. 1, reportedly following a 1st order low-pass response [3].

The m-HSCAP signal is generated following the block diagram in Fig. 2. At the transmitter, the super-Nyquist and orthogonal SBs are generated as two separate entities. First, m independent data streams from $\mathbf{D_1}$ to $\mathbf{D_m}$ are generated, which are then mapped onto the 4-level quadrature amplitude modulation (QAM) constellation before being split into their in-phase ($s(t)$) and quadrature components ($\overline{s}(t)$)), followed by up-sampling via
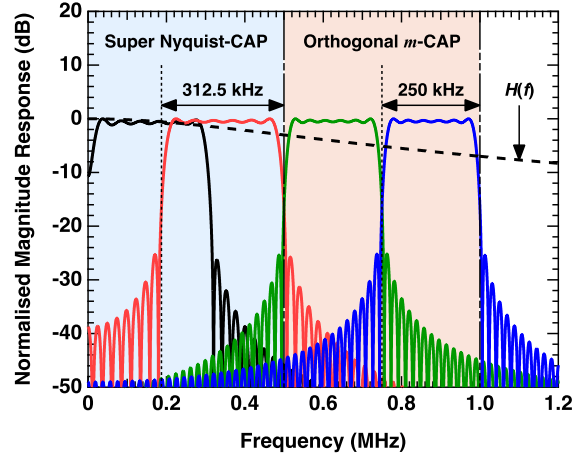

Fig. 1. Conceptual frequency response of the proposed hybrid modulation format

zero-padding. The total baud rate for the super-Nyquist R_{sN} system is given by:

$$R_{sN} = \frac{B_N}{(1 + \beta)(1 - \alpha)} \quad (1)$$

where B_N is the portion of the signal bandwidth B_{sig} dedicated to the non-orthogonal SBs, β is the excess bandwidth factor of the pulse shaping filters and α is the bandwidth expansion factor, which controls the increase in R_{sN}. For the orthogonal part, the symbol rate R_{sO} is given by:

$$R_{sO} = \frac{B_{sig} - B_N}{1 + \beta} \quad (2)$$

Note, the number of samples-per-symbol N_{SS} controls the sampling frequency f_s for each part of the system. The nature of m-HSCAP, where two different symbol rates are essentially being transmitted, means that the scheme must be multi-rate until the point of SB aggregation (see the modulator in Fig. 2). In both cases, for up-sampling we have [6]:

$$N_{SS} = \gamma \lceil 2m(1 + \beta) \rceil \quad (3)$$

where γ is an over-sampling factor set to 4 in this work without any loss of generality.

After up-sampling, the data streams are then passed through the pulse shaping filters, usually given as the product of a square-root raised cosine (SRRC) $g(t)$ with excess bandwidth β and a cosine/sine wave pair [14]. The ith in-phase $p_i(t)$ and imaginary $\overline{p_i}(t)$ pulse shaping filter for either entity are [14]:

$$p_i(t) = g(t)\cos(2\pi f_i t) \quad (4)$$
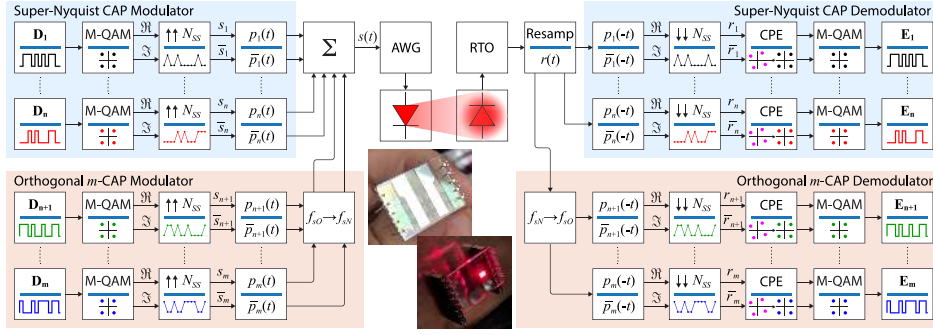
$$\overline{p_i}(t) = g(t)\sin(2\pi f_i t) \quad (5)$$

Fig. 2. Simplified block diagram for the proposed m-HSCAP scheme; inset shows two PLEDs used

where f_i is the carrier frequency of ith sub-carrier given as:

$$f_i = \begin{cases} \dfrac{B_{N\min}}{2} + \dfrac{i\,(1 - B_{N\min})}{n - 1} & i \in \{1, \ldots, n\} \\[2ex] B_N + \dfrac{B_{\min}\,(2i - 1)}{2} & i \in \{n + 1, \ldots, m\} \end{cases}$$

(6)

where n is the number of SBs assigned to the super-Nyquist part, $B_{N\min}$ is the minimum bandwidth occupied by a single non-orthogonal SB with R_{sN} and $B_{\min}$ is the bandwidth occupied by an orthogonal SB with R_{sO}. Note, the mathematical details on pulse shapes are widely documented [14].

As mentioned, at the point of pulse shape filtering the system is multi-rate for any value of $\alpha > 0$. Thus, two different relationships define the the minimum sampling frequency that satisfies the Nyquist rate. For the super-Nyquist part, the minimum sampling frequency is given by:

$$f_{sN} = \frac{R_{sN} N_{SS}}{n}$$

(7)

while the orthogonal part is given by:

$$f_{sO} = \frac{R_{sO} N_{SS}}{m - n}$$

(8)

Clearly, $f_{sN} > f_{sO}$ is a constant condition for this scheme except for the special case of no expansion (i.e. $\alpha = 0$), where $f_{sN} = f_{sO}$. Therefore, it is necessary to resample the orthogonal entity from $f_{sO} \longrightarrow f_{sN}$ before summation, where each sample must be transmitted at the same rate. After resampling, the two entities are directly summed for transmission as [6, 14]:

$$s(t) = \sum_{i=1}^{m} \left[s_i(t) \otimes p_i(t) - \overline{s_i}(t) \otimes \overline{p_i}(t) \right]$$

(9)

which results in the superposed spectrum, see Fig. 3. Note the $\sim$6 dB power penalty, which is dependent on both n and β as reported in [12].

The entire physical setup is controlled and automated using LabVIEW to ensure equivalent test conditions for all signals under test. The generated signal $s(t)$ is then loaded into a Tektronix AWG70002A arbitrary waveform generator (AWG), with 4 GHz analogue bandwidth and 10-bit vertical resolution, the output of which is used for intensity modulation of PLED via a $4\times$ amplifier (TI THS3202) and a custom-built driver which supplies 20 mA dc and 20 mA ac currents.

B. PLED Fabrication and Characterisation

PLEDs used here were fabricated using oxygen plasma treated indium tin oxide (ITO) substrates as transparent anodes (OSSILA Ltd) [15]. On top of these, a 40 nm poly(3,4-ethylenedioxythiophene)-poly(styrenesulfonate) (PEDOT:PSS) hole-injection layer was deposited via spin coating from a water dispersion (Heraeus Clevios AI 4083) in air and annealed at 150°C for 10 minutes in a nitrogen-filled glove-box. Following this, the active polymer (PIDT-2TPD, number average molecular weight = 63.7 kDa, polydispersity index = 2.3), whose chemical structure and synthesis were reported in [16, 17], was deposited via spin-coating from a toluene solution, following the same protocol used in [18]. Finally, a calcium/aluminium (Ca/Al with thicknesses of 30 and 200 nm, respectively) cathode was thermally evaporated on top, to obtain, for each substrate, six independent
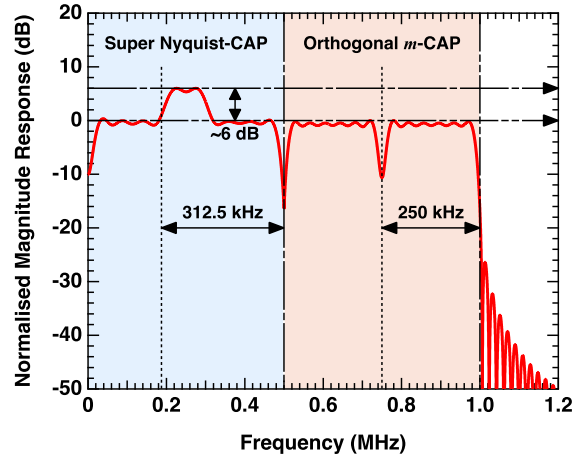

Fig. 3. Superposed ideal magnitude response of the proposed hybrid scheme

pixels with an active area of 4.5 mm^2, as defined by the overlap between the patterns of the ITO anode and the Ca/Al cathode. To prevent oxidation of the Ca and the emissive polymer layers, therefore preserving the device stability when operated in air, each PLED was encapsulated by covering the active area and metal electrodes with a layer of epoxy resin (OSSILA Ltd) and a protective glass slide. The resin was then cured by exposing the PLEDs to UV light for 15 minutes in the glovebox, see photos inset in Fig. 2.

The current-voltage (I-V) and current-optical power density (I-L) relationships were measured using a Keithley 2400 source-meter for dc power supply and a calibrated photodetector and are illustrated as an L-I-V curve in Fig. 4, which also shows the operating conditions for intensity modulation. The PLED has a clear pseudo-linear operating region over the ac current range selected, as highlighted by the linear fit $L_{\text{fit}} = 330.72 I_{\text{dc}} - 1.5698$, where I_{dc} (A) is the drive current. The emission spectrum is depicted inset in Fig. 4 showing strong red emission with a peak at 639 nm and two shoulders in the near-infrared region with peaks at ∼688 nm and ∼760 nm originating from weaker vibronic transitions. A single 4.5 mm^2 PLED pixel and a link distance of 5 cm are adopted for consistency with previous work [3, 19] and to avoid excessive power burden on the device. The measured PLED bandwidth is ∼500 kHz as illustrated by $H(f)$ in Fig. 1 and [19], which shows the rise time equivalent.

C. Hybrid Multi-Band CAP Demodulator

At the receiver, a photodetector (Thorlabs PDA36A2, composed of a 12 MHz photodiode and transimpedance amplifier) and a 20 dB amplifier are used to regenerate the electrical signal, which is captured using an 8 GHz Tektronix MSO70804C real time oscilloscope (RTO) at 62.5 MS/s.

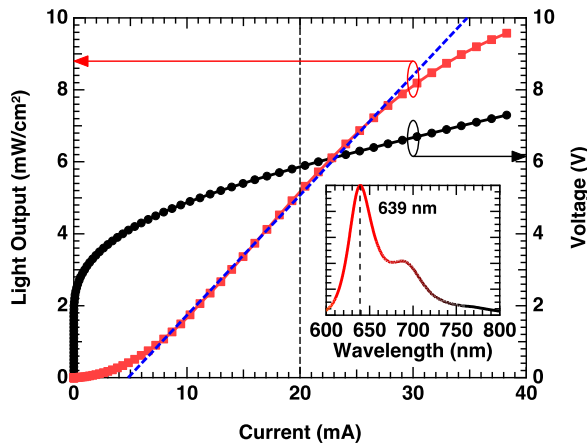Next, the sampled signals are processed in MATLAB beginning with resampling to the original transmit rate

of f_{sN}. The signals are then passed through a 4$^{\text{th}}$ order low-pass filter (not shown in Fig. 2) to remove out-of-band noise. This is followed by splitting the signal into their original super-Nyquist and orthogonal entities. For super-Nyquist, the signal is passed through a time-reversed matched filter pair, which effectively band-pass filters the in-phase and quadrature components for each SB, before down-sampling at a rate of N_{SS}. Next, the common phase error (CPE) is removed using conventional techniques reported widely in [20] before constellation de-mapping and estimation of the transmitted bits $\mathbf{E_i}$ for the ith channel. For orthogonal SBs, the process is identical except for an additional resampling performed before matched filtering to recover the original sampling rate of the signal before transmission, recalling that $f_{sO} \neq f_{sN}$ when $\alpha > 0$. A minimum of 10^{-6} bits are captured for each SB and the root mean square error vector magnitude (EVM$_{\text{RMS}}$) is measured for every SB.

III. RESULTS

The measured EVM$_{\text{RMS}}$ of m-HSCAP for $\beta = 0.5$ is illustrated in Fig. 5 for $m = \{10, 8, 6 \text{ and } 4\}$. In each case, half of the SBs exist in the non-orthogonal region (dashed lines) and the rest in the orthogonal region (solid lines) of the signal bandwidth. As shown in Fig. 5 it is clear in every case that, orthogonal signals in the stopband of $H(f)$ can be supported with an EVM$_{\text{RMS}}$ in the range of 10-20% with a loose dependence on the number of SBs used. This is counter intuitive as it is expected, based on the literature [8], that the EVM$_{\text{RMS}}$ decreases with increasing m. Therefore, we attribute this to the increased peak-to-average power ratio (PAPR) associated with higher orders of m, thus causing a limitation on the received signal-to-noise ratio [21]. Furthermore, the EVM$_{\text{RMS}}$ increases with the carrier frequencies of the
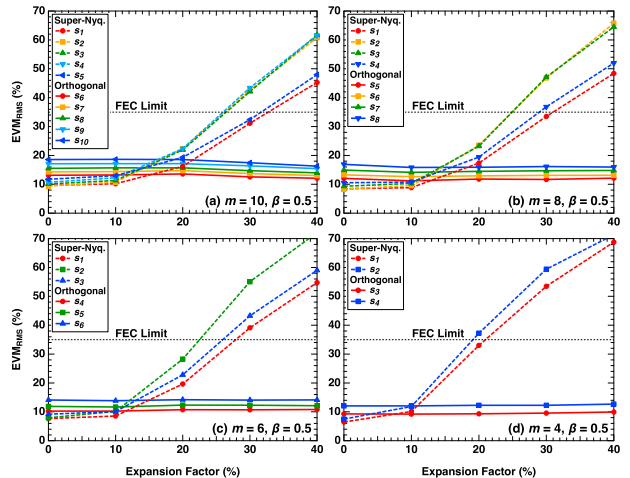
Fig. 5. EVM$_{\text{RMS}}$ measurements for both the orthogonal (solid lines) and super-Nyquist (dashed) for the $s_i{}^{\text{th}}$ sub-band, $\beta = 0.5$ and (a) $m = 10$, (b) $m = 8$, (c) $m = 6$ and (d) $m = 4$

Fig. 4. Measured L-I-V curve of the PLED under test. Inset: measured electroluminescence spectrum measured at the operating point

orthogonal SB, due to the increased attenuation experienced.

In terms of the non-orthogonal SBs located inside the PLED modulation bandwidth, it is clear that EVM_{RMS} experienced for a higher number of sub-bands is lower, i.e. for $\alpha = 20\%$, the average EVM_{RMS} values are $\sim 20\%$ and 35% for $m = 10$ and 4, respectively. This is because of a combination of the reduced SB bandwidth and increased excess energy (i.e. $\beta = 0.5$) in the pulse-shaping filters. Note, increasing m results in reduced relative overlap between the super-Nyquist SBs [12]. Hence, when combined with the additional excess energy provided for high β, IBI is reduced and therefore high-order systems can tolerate an increased level of expansion at lower values of EVM_{RMS}. This is supported by the fact that for higher values of m the EVM_{RMS} drops well below the threshold level of $\sim 35\%$ (corresponding to a 7% forward error correction (FEC) BER limit of $3.8 \times 10{-3}$).

The mean EVM_{RMS} shown in Fig. 6 reveals that higher expansion can be supported with aggregate error rates below the FEC limit, and in principle should be supported by up to $\sim 25\%$ for $m \geq 6$. This agrees with literature reported on super-Nyquist CAP systems where up to 30% of bandwidth can be saved when used in a compressive mode, i.e. where the overall signal bandwidth is reduced, and the baud rate is not increased [12]. It is also indicated that limited improvement is achieved by increasing the number of SBs since there is limited improvement in EVM_{RMS} for $m > 8$. This is also in good agreement with the literature, which shows the benefits of m-CAP plateau beyond a given number of sub-bands depending on the system being adopted [8, 22].

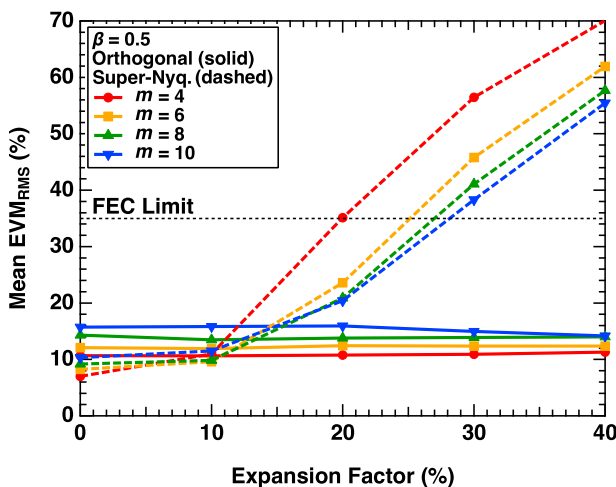In terms of overall throughput, for m-HSCAP the total bit rate $R_{bT} 1.5$ Mb/s (using (1) and (2)) for $\beta = 0.5$, $\alpha = 20\%$ and 4-QAM (and $m > 4$). Under the same conditions, m-HSCAP offers throughput improvements of $\sim 67\%$ and 12% compared to m-SCAP (with R_{sN} of ~ 450 kbaud (900 kb/s) and B_{mod} of 500 kHz) and m-CAP (with R_{sT} of ~ 667 kbaud (1333 kb/s) and B_{sig} of 1 MHz), respectively. Similar analysis is performed for the same system but for lower energy levels in the guard band, i.e., $\beta = 0/1$. The full EVM_{RMS} results as a function of the expansion factor are presented in Fig. 7. For the orthogonal case, the EVM_{RMS} levels are almost constant for the range of m, but are reduced by an average of 4% compared to Fig. 5. The reason for this is that lower β requires a higher number of filter-taps to achieve the equivalent EVM_{RMS} (or BER) [14]. In this work, we kept the number of filter-taps constant to maintain a constant computational load, as is the general case in m-CAP with different values of β [12, 14]. For the super-Nyquist SBs with a similar trend as in Fig. 5, albeit at a lower α than previously experienced, the EVM_{RMS} values below the FEC limit are within the expansion range of 10-15% compared to 20-30% in Fig. 5. This is because of overlapping SBs, due to the reduced excess energy (i.e., lower β), where IBI induced degradation on the signal constellation prior to demodulation is more significant, thus resulting in higher BERs.

Finally, in Fig. 8 the measured mean EVM_{RMS} against the expansion factor for a range of m and β of 0.1 is illustrated. The variation between measurements is clearly reduced in comparison to Fig. 6. Note from observation of Figs. 6 and . 8, β is the key parameter in m-HSCAP, which influences the achievable α and the number of SBs that can be used in the super-Nyquist case. In addition, clearly a higher rate, which is proportional to the sum of (1) and (2), can be achieved with a larger number of SBs (i.e. up to $m = 10$) for
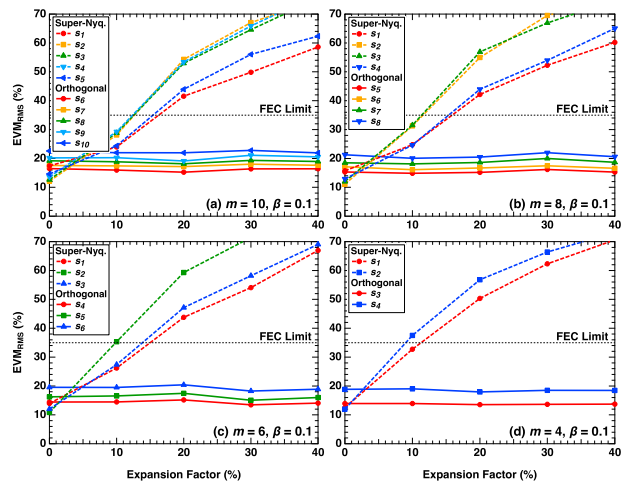

Fig. 6. Mean EVM_{RMS} dependance on the expansion factor ($\beta = 0.5$)

Fig. 7. EVM_{RMS} measurements for both the orthogonal (solid lines) and super-Nyquist (dashed) for the s_ith sub-band, $\beta = 0.1$ and (a) $m = 10$, (b) $m = 8$, (c) $m = 6$ and (d) $m = 4$
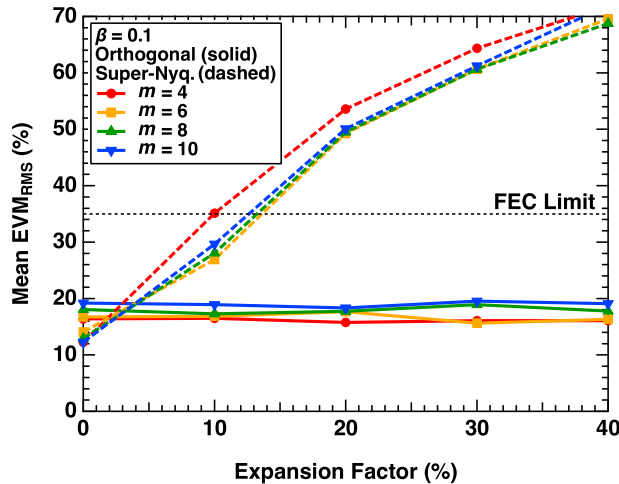
Fig. 8. Mean EVM$_{RMS}$ dependence on the expansion factor ($\beta = 0.1$)

$\beta = 0.5$, since a higher α can be reached considering the mean EVM$_{RMS}$. However, for $\beta = 0.1$ (i.e. Fig. 8), there is little difference between the case where $m = 6$ to 10. This could be used to advantageously design the signal to remove computational complexity via removing filters from the system structure altogether. In terms of throughput, m-HSCAP can support an overall bit rate of 1.92 Mb/s, following (1) and (2) for $\beta = 0.1$, $\alpha = 10\%$ and 4-QAM. Using the same method as previous, we calculated that m-SCAP and conventional m-CAP can deliver bit rates of $\sim$1 Mb/s and 1.8 Mb/s, respectively which corresponds to improvements of $\sim$90% and 7%, respectively.

IV. CONCLUSION

In this work, we proposed a hybrid modulation format, which improved the throughput of both m-SCAP and conventional m-CAP systems by up to 90% and 7%, respectively. We showed that for orthogonal signals in the stop-band of PLED the measured EVM$_{RMS}$ were in the range of 10-20% with a loose dependence on the number of SBs, whereas for the non-orthogonal signals located within pass-band of PLED the average EVMRMS were $\sim$20% and 35% for $m = 10$ and 4, respectively.

REFERENCES

[1] A. Burton, H. Le Minh, Z. Ghassemlooy *et al.*, "Experimental demonstration of 50-Mb/s visible light communications using 4×4 MIMO," *IEEE Photonics Technology Letters*, vol. 26, no. 9, pp. 945–948, 2014.
[2] S. H. Shao, A. Khreishah, M. Ayyash *et al.*, "Design and analysis of a visible-light-communication enhanced WiFi system," *Journal of Optical Communications and Networking*, vol. 7, no. 10, pp. 960–973, 2015.
[3] P. A. Haigh, F. Bausi, H. Le Minh *et al.*, "Wavelength-multiplexed polymer LEDs: Towards 55 Mb/s organic visible light communications," *IEEE Journal on Selected Areas in Communications*, vol. 33, no. 9, pp. 1819–1828, 2015.
[4] P. A. Haigh, F. Bausi, Z. Ghassemlooy *et al.*, "Visible light communications: real time 10 Mb/s link with a low bandwidth polymer light-emitting diode," *Opt Express*, vol. 22, no. 3, pp. 2830–8, 2014.
[5] J. Wang, Y. Xu, X. Ling *et al.*, "PAPR analysis for OFDM visible light communication," *Optics express*, vol. 24, no. 24, pp. 27 457–27 474, 2016.
[6] M. I. Olmedo, T. J. Zuo, J. B. Jensen *et al.*, "Multiband carrierless amplitude phase modulation for high capacity optical data links," *Journal of Lightwave Technology*, vol. 32, no. 4, pp. 798–804, 2014.
[7] F. M. Wu, C. T. Lin, C. C. Wei *et al.*, "Performance comparison of OFDM signal and CAP signal over high capacity RGB-LED-Based WDM visible light communication," *IEEE Photonics Journal*, vol. 5, no. 4, pp. 7 901 507–7 901 507, 2013.
[8] P. A. Haigh, A. Burton, K. Werfli *et al.*, "A multi-cap visible-light communications system with 4.85-b/s/Hz spectral efficiency," *IEEE Journal on Selected Areas in Communications*, vol. 33, no. 9, pp. 1771–1779, 2015.
[9] P. A. Haigh, S. T. Le, S. Zvanovec *et al.*, "Multi-band carrier-less amplitude and phase modulation for bandlimited visible light communications systems," *IEEE Wireless Communications*, vol. 22, no. 2, pp. 46–53, April 2015.
[10] Y. Wang, Y. Zhou, T. Gui *et al.*, "Efficient MMSE-SQRD-based MIMO decoder for SEFDM-based 2.4-Gb/s-spectrum-compressed WDM VLC system," *IEEE Photonics Journal*, vol. 8, no. 4, pp. 1–9, 2016.
[11] S. Liang, Z. Jiang, L. Qiao *et al.*, "Faster-than-Nyquist precoded CAP modulation visible light communication system based on nonlinear weighted look-up table predistortion," *IEEE Photonics Journal*, vol. 10, no. 1, pp. 1–9, 2018.
[12] P. Haigh, P. Chvojka, Z. Ghassemlooy *et al.*, "Visible light communications: multi-band super-Nyquist CAP modulation," *Optics Express*, vol. 27, no. 6, pp. 8912–8919, 2019.
[13] Y. Wang, X. Huang, L. Tao *et al.*, "4.5-Gb/s RGB-LED based WDM visible light communication system employing CAP modulation and RLS based adaptive equalization," *Optics express*, vol. 23, no. 10, pp. 13 626–13 633, 2015.
[14] P. Chvojka, K. Werfli, S. Zvanovec *et al.*, "On the m-CAP performance with different pulse shaping filters parameters for visible light communications," *IEEE Photonics Journal*, vol. 9, no. 5, pp. 1–12, 2017.
[15] T. M. Brown, G. M. Lazzerini, L. J. Parrott *et al.*, "Time dependence and freezing-in of the electrode oxygen plasma-induced work function enhancement in polymer semiconductor heterostructures," *Organic Electronics*, vol. 12, no. 4, pp. 623–633, 2011.
[16] A. Minotto, P. Murto, Z. Genene *et al.*, "Efficient near-infrared electroluminescence at 840 nm with "Metal-Free" Small-Molecule:Polymer Blends," *Adv Mater*, vol. 30, no. 34, p. e1706584, 2018.
[17] P. Murto, Z. Genene, C. M. Benavides *et al.*, "High performance all-polymer photodetector comprising a donor–acceptor–acceptor structured indacenodithiophene–bithieno [3, 4-c] pyrroletetrone copolymer," *ACS Macro Letters*, vol. 7, no. 4, pp. 395–400, 2018.
[18] A. Zampetti, A. Minotto, B. M. Squeo *et al.*, "Highly efficient solid-state near-infrared organic light-emitting diodes incorporating ADA dyes based on α, β-unsubstituted "BODIPY" moieties," *Scientific reports*, vol. 7, no. 1, p. 1611, 2017.
[19] P. A. Haigh, A. Minotto, A. Burton *et al.*, "Experimental demonstration of staggered CAP modulation for low bandwidth red-emitting polymer-LED based visible light communications," *arXiv preprint arXiv:1234:56789*, 2019.
[20] S. T. Le, P. A. Haigh, A. D. Ellis *et al.*, "Blind phase noise estimation for CO-OFDM transmissions," *Journal of Lightwave Technology*, vol. 34, no. 2, pp. 745–753, 2016.
[21] M.-A. Khalighi, S. Long, S. Bourennane *et al.*, "PAM-and CAP-based transmission schemes for visible-light communications," *IEEE Access*, vol. 5, pp. 27 002–27 013, 2017.
[22] P. A. Haigh, E. Hugues-Salas, and J. Wei, "On the performance of increasing subcarrier order in multi-band carrier-less amplitude and phase modulation for short haul optical links," in *Asia Communications and Photonics Conference.* Optical Society of America, 2017, pp. S4B–6.